

The importance of liquid evaporation on rectified diffusion processes

D. Fuster^{*} and S. Zaleski[†]

^{*} Division of Engineering and Applied Science, California Institute of Technology, Pasadena, California 91125, USA

[†] UPMC Univ Paris 06, UMR 7190, Institut Jean Le Rond d'Alembert, F-75005 Paris, France.

fuster@caltech.edu and zaleski@lmm.jussieu.fr

Keywords: Rectified diffusion, mass transfer, phase diagrams, lithotripsy

Abstract

This paper unveils the basic mechanisms underlying rectified diffusion processes. The exact solution of the radial transport of species in both phases, gas and liquid, turns to be crucial to accurately predict the growth rate in the context of lithotripsy. The Direct Numerical Simulation of the temporal evolution of a spherical bubble is used to gain new insight on the effect of two phenomena: Transient effects related with the gas diffusion in the liquid and non uniform concentration gradients inside the bubble. The special characteristics of the process impedes a direct application of usual hypothesis usually applied in studies related with bubble growth in ultrasonic fields.

Nomenclature

Roman symbols

D	diffusion coefficient (m^2s^{-1})
e	internal energy (Jkg^{-1})
h	enthalpy (Jkg^{-1})
j	flux ($\text{kgm}^{-2}\text{s}^{-1}$)
J	Total mass flux ($\text{kgm}^{-2}\text{s}^{-1}$)
N	Number of species(–)
p	pressure (Nm^{-2})
q	heat flux (Jm^{-2})
r	radial coordinate (m)
R	bubble radius (m)
R_g	gas universal constant ($\text{Jkg}^{-1}\text{K}^{-1}$)
\dot{R}	interface velocity (ms^{-1})
t	time (s)
T	Temperature (K)
v	fluid velocity (ms^{-1})
W	molecular weight (molkg^{-1})
z	decaying coefficient (s^{-1})
Y	mass fraction (kgkg^{-1})

Greek symbols

α	species name(–)
β	accommodation coefficient(–)
Δ	Increment (–)
δ	Boundary layer thickness (m)
ϕ	viscous dissipation ($\text{Jm}^{-3}\text{s}^{-1}$)
η	mass loading (–)
κ	thermal conductivity ($\text{Wm}^{-1}\text{K}^{-1}$)

μ	viscosity ($\text{kgm}^{-2}\text{s}^{-1}$)
ρ	Density (kgm^{-3})
σ	surface tension (Nm^{-1})
τ	viscous stresses (Nm^{-2})
ω	angular frequency (rads^{-1})

Subscripts

c	characteristic
f	final
g	gas
i	interface
l	liquid
max	maximum
o	initial
r	radial component
ref	reference

Superscripts

diff	diffusion
dis	disequilibrium
p	Particle
sat	saturation
*	Nondimensional number

Introduction

The phenomenon of rectified diffusion in oscillating bubbles has been widely studied during the past two decades. When a bubble expands and its pressure decreases, part of the gas dissolved into the liquid

is transferred to the bubble. When the bubble is compressed, the gas contained inside the bubble is re-dissolved in the liquid. Naively we could think that for weak oscillations these effects would balance over a cycle. However, non-linear effects associated with the mass transfer processes can lead to a net gas intake that makes the bubble grow significantly even over a single cycle (Blake Jr 1949). The larger area of the bubble during the expansion, when the gas enters the bubble, and the stretching of the gas boundary layer during this stage are the two main mechanisms responsible for this bubble growth (Brennen 1995).

In ultrasonic applications, where the bubble is steadily oscillating for hours, two different time scales are present. One is the excitation period which determines how the bubble behaves mechanically during one cycle, the other one is the timescale associated with gas diffusion from the bubble interface into the liquid. Typical values of the short timescale are of the order of tens of microseconds, whereas the second one occurs on much longer time scales, typically, on the order of minutes (Crum 1980; Eller 1969). However, this distinction does not apply to all the processes involving rectified diffusion. In shock wave lithotripsy (Cunningham et al. 2001; Church 1988), the bubble expands and collapses in response to an incoming pressure wave, which is repeated with a frequency between 1 and 100 Hz. In this case, the bubble mass can be significantly increased during the pass of the shock wave but it slowly tends to be dissolved until the next shock wave arrives.

Different theories and models have been developed to describe both bubble dynamics and the mass transfer processes across the interface. The early models proposed by Hsieh and Plesset (1961) and by Eller and Flynn (1965), as well as later improvements proposed by Crum (1980), solve the diffusion problem from a pure gas bubble into the surrounding liquid. Using the proper time averages during one cycle to obtain the average concentration at the interface, these theories solve analytically the diffusion equation in the liquid to obtain expressions for the cavitation threshold and growth rate for the radius of gas bubbles. More recently, Lohse et al. (Toegel and Lohse 2003; Hilgenfeldt et al. 1996) have used similar models to predict the stability of bubbles in single bubble sonoluminescence, where the equilibrium radius is governed by a very slow mass transfer process. Also, Fyrrillas and Szeri (1994) have improved previous theories for the prediction of the growth rate of bubble radius.

All theories resort to simplifications that can be unacceptable in some situations. In this work, a complete

model based on Hauke et al. (2007) is extended in order to investigate the processes underlying mass transfer in applications where rectified diffusion is important. The gas intake of a bubble is shown to be sensitive to the bubble radius evolution and the transport of species in each of the phases. In those situations where the liquid pressure falls below the liquid vapor pressure, an intense evaporation is produced, significantly influencing both the transport of species across the interface and also the bubble radius evolution. Thus, the inclusion in the model of mass transfer effects across the interface along with the diffusion equation of gas in the liquid coupled with the diffusion equation inside the bubble is needed to obtain an accurate prediction the net gas intake.

In the first part of the paper, the basic equations are presented. Based on these equations, different simplifications are discussed in order to solve the Navier-Stokes equations inside and outside the bubble coupled with the energy and species diffusion equations. Finally, the numerical results are used to scrutinize the importance of different mechanisms on rectified diffusion.

1 Governing equations

1.1 Conservation Laws

The time-dependent dynamics of a single bubble and its surrounding liquid assuming spherical symmetry are governed by the following set of partial differential equations

$$\frac{D\rho}{Dt} + \frac{\rho}{r^2} \frac{\partial(v_r r^2)}{\partial r} = 0, \quad (1)$$

$$\rho \frac{DY_\alpha}{Dt} = -\frac{1}{r^2} \frac{\partial}{\partial r} \left(r^2 j_\alpha^{\text{diff}} \right), \quad (2)$$

$$\rho \frac{Dv_r}{Dt} = -\frac{\partial p}{\partial r} + \frac{1}{r^2} \frac{\partial}{\partial r} (r^2 \tau_{rr}), \quad (3)$$

$$\rho \frac{De}{Dt} = -p \nabla \cdot \mathbf{v} - \frac{1}{r^2} \frac{\partial(r^2 q_r)}{\partial r} + \phi_v, \quad (4)$$

where $\frac{D}{Dt}$ represents the substantial derivative,

$$\frac{D}{Dt} = \frac{\partial}{\partial t} + v \frac{\partial}{\partial r},$$

The notations used are defined in the Nomenclature.

The system defined by Eqs. (1-4) is supplemented by a state equation that relates the thermodynamic properties, an equation describing the rheology of the fluid and a law for the diffusive mass flux. As these equations depend on the model applied, they are described later.

1.2 Boundary conditions

In order to solve the system of equations presented above, symmetry conditions are established at the bubble center. Far from the bubble, we assume that the bubble has no effect on the liquid temperature and concentration, which considered to be constants T_∞ and $Y_{\alpha,\infty}$, respectively.

The pressure is spatially uniform in the bubble far field. The expression for its temporal evolution is given in the examples.

At the interface we can apply local balances to relate the variables on both sides. The continuity condition establishes a relation between the net mass flux across the interface, J , the interface velocity \dot{R} , and the gas and liquid velocities at the interface, $v_g(R, t)$ and $v_l(R, t)$

$$J = \rho_g [v_g(R, t) - \dot{R}] = \rho_l [v_l(R, t) - \dot{R}]. \quad (5)$$

Analogously, we can apply the continuity condition to every species. The total flux of species α across the interface, j_α , is the sum of the advective flux related with the mass exchange across the interface, $j_\alpha^{\text{adv}} = JY_{\text{int},\alpha}$, and the diffusive flux, j_α^{diff}

$$j_\alpha = JY_\alpha^l - \rho_l D_\alpha^l \frac{\partial Y_\alpha^l}{\partial r} = JY_\alpha^g - \rho_g D_\alpha^g \frac{\partial Y_\alpha^g}{\partial r}, \quad (6)$$

where the total flux of mass across the interface is

$$J = \sum_\alpha j_\alpha. \quad (7)$$

In order to relate the pressures at both sides of the interface, the momentum balance at $r = R(t)$ yields (Yasui 1997; Sochard et al. 1998)

$$p_g = p_l + \frac{4\mu_l \dot{R}}{R} + \frac{2\sigma}{R} + J^2 \left(\frac{1}{\rho_l} - \frac{1}{\rho_g} \right) \quad (8)$$

where the gas viscous stresses and liquid compressibility have been neglected.

The heat balance at the interface establishes the relation among the heat fluxes in the liquid and gas sides

$$\begin{aligned} -\kappa_l \frac{\partial T_l}{\partial r} + (v_l - \dot{R})\rho_l h_l - \rho_l \sum_{\alpha=1}^N h_\alpha^l D_\alpha^l \frac{\partial Y_\alpha^l}{\partial r} = \\ -\kappa_g \frac{\partial T_g}{\partial r} + (v_g - \dot{R})\rho_g h_g - \rho_g \sum_{\alpha=1}^N h_\alpha^g D_\alpha^g \frac{\partial Y_\alpha^g}{\partial r}, \quad (9) \end{aligned}$$

and finally, a continuous temperature profile across the interface is assumed

$$T_g = T_l, \quad r = R(t). \quad (10)$$

The spatial boundary conditions required to solve the set of PDE is completed by establishing another relation at the interface. Previous models developed for the study of SBSL have applied models based on the kinetic theory of gases to relate the flux across the interface with the instantaneous conditions (Yasui 1997; Storey and Szeri 2000), details about the model implemented to obtain the results included in this work are contained in Section 2. However the experimental validation of these models in different conditions is difficult and accurate values of the coefficients appearing in the model that should be experimentally measured are unknown (e.g. accommodation coefficient). As an alternative, we can avoid the use of a mass transfer model by assuming that equilibrium conditions prevail at the interface at every moment. This hypothesis is especially suitable for weak oscillations when the conditions at the interface do not reach supercritical conditions and the disequilibrium encountered at the interface is expected to be negligible. To assume equilibrium conditions at the interface implies that the uncertainty due to the evaporation model is avoided. From dimensional analysis, this assumption seems to be valid for weak amplitudes, irrespective of the frequency, or low frequencies. Further details about this analysis and numerical validation are currently under preparation. For the case of water, the partial water pressure is related with the interface temperature and pressure by means of the Clausius–Clapeyron equation. For soluble gases, Henry’s law can be used to relate the concentrations across the interface.

Initial conditions

In order to specify the initial conditions it is assumed that the bubble is initially in mechanical equilibrium with the surrounding liquid. This implies that the initial interface velocity is zero ($\dot{R} = 0$), the bubble temperature is constant and equal to the liquid temperature, and the initial fluid velocities are zero. The liquid pressure far away from the bubble, p_∞ , is given, so the initial internal bubble pressure can be calculated by means of the momentum balance at the interface from Eq. (8). The initial gas density can be calculated from the bubble pressure and temperature. Finally, the initial water concentration is given by the equilibrium conditions. In the cases presented in this work, only binary mixtures composed of a volatile liquid and an partially soluble gas are considered. The liquid vapor pressure determines the concentration of gas and vapor inside the

bubble. At the same time, the gas concentration inside the bubble determines the concentration of gas at the interface.

Surface tension effects induce a concentration gradient between the bubble interface and the liquid bulk so that the bubble tends to dissolve. The correct initial concentration profile in the liquid is not clear. In this work, we assume that the concentration profile in the liquid comes from the steady-state solution of the species equations.

2 Model

In this work a model based on the one presented in Hauke et al. (2007) is used. This model resorts to the Rayleigh-Plesset equation with the additional compressibility terms of Keller and Miksis (1980). This equation is used to work out the bubble radius evolution as a function of the forcing pressure wave.

The model is extended in order to include mass transfer phenomena inside and outside the bubble. The radial diffusive heat and mass fluxes follow the Fourier and Fick's laws, respectively,

$$q_r = -\kappa \frac{\partial T}{\partial r} + \sum_{\alpha=1}^N j_{\alpha}^{\text{diff}} h_{\alpha}, \quad (11)$$

$$j_{\alpha}^{\text{diff}} = -\rho D_{\alpha} \frac{\partial Y_{\alpha}}{\partial r}, \quad (12)$$

At large frequencies, mass transfer effects can be important and the equilibrium hypothesis is questionable. However in this paper we neglect non equilibrium effects and thus apply the equilibrium conditions at the interface for the gas concentration (Henry's law) and partial pressure and the water vapor. In other words the gas is considered as a partially soluble substance.

3 Numerical method

As pointed out by Hao and Prosperetti (Hao and Prosperetti 1999), special care must be taken when the complete Navier-Stokes equations are coupled with the equations describing the mass transport inside the bubble and in the liquid. In this section, we present a consistent method to solve the equations presented above. We summarize the method in the form of an algorithm

1. Consider an instant t in which the solution is known (\mathbf{Y}^t)

$$\mathbf{Y} = (R, \rho_g, \mathbf{u}_g, T_g, \mathbf{Y}_{\alpha,g}, T_l), \quad (13)$$

As an initial guess, for the solution at $t + \Delta t$, all the required variables are extrapolated using a forward Euler step

$$\mathbf{Y}_{n+1}^{t+\Delta t} = \mathbf{Y}_n^t + \Delta t \cdot \dot{\mathbf{Y}}_n^t, \quad (14)$$

where the subscript n denotes the iteration number.

2. The net gas mass flux, J_{gas} , across the interface at $t + \Delta t$ is obtained. This flux is directly given by the local balance at the interface (Eq. 6), the concentration field estimated at $t + \Delta t$ and the total mass flux (J).
3. The interface velocity and acceleration are found from the Rayleigh-Plesset equation. In this equation, the acceleration appears (\dot{R}_b) and as a consequence the interface velocity (\dot{R}_b) is treated as an unknown variable that is integrated with a backward Euler method.
Once the interface velocity is known, the velocity field inside the bubble is assumed to be linear whereas the velocity field in the liquid is worked out based on the incompressibility hypothesis.
4. The system of differential equations consisting of the continuity, species and energy equation in both phases (Eqs. 1-4) is segregated. Every equation is discretized in space using a Finite Element Method (FEM). The system of equations constitute a tridiagonal system which can be solved by encoding efficiently the procedure for the LU decomposition (Press et al. 1992). This method saves a substantial amount of time in comparison with more complex techniques.

An Arbitrary Lagrangian Eulerian (ALE) formulation allow us to move the mesh independently and to track the interface at every moment. The mesh node position at $t + \Delta t$ is updated using the velocity $u^{m,t+\Delta t}$ which is evaluated as

$$u^{m,t+\Delta t} = \begin{cases} \dot{R}_b \left(\frac{r}{R_b} \right) & r \leq R(t) \\ \dot{R}_b \left(\frac{R_b}{r} \right)^2 & r > R. \end{cases} \quad (15)$$

The mesh is initially adapted concentrating the nodes near the interface, where the larger gradients must be well resolved in order to correctly predict the heat and mass transfer across the interface.

With the new mesh, the segregated method proceeds as follows.

- a) The species equations inside the bubble (Eq. 2) is solved for the vapor $Y_{\alpha,g}^{t+\Delta t}$. Zero derivative is imposed at the bubble center whereas at the interface two different boundary conditions are considered. When transient effects are taken into account, the total vapor flux obtained from the Hertz-Knudsen-Langmuir equation is imposed.
 - b) The diffusion equation for the partially soluble gas is solved in the liquid domain. Dirichlet boundary conditions are imposed at both boundaries; the concentration at the interface is given by the Henry's law and the concentration at infinity is assumed to be known.
 - c) The equation in both phases, liquid and gas, is coupled using the heat balance at the interface (Eq. 9). Symmetry at the bubble center and the temperature at infinity are imposed.
5. The convergence error is then obtained from comparison of the initial guess and the updated values. At the n iteration step, we take the maximum of the convergence error of all the variables considered in the problem

$$\epsilon = \max \left(\frac{Y_{n+1}^{t+\Delta t} - Y_n^{t+\Delta t}}{Y_n^{t+\Delta t}} \right) \quad (16)$$

If ϵ is larger than a given tolerance tol , a new iteration starts in step 3. If after n_{\max} iterations ($n_{\max}=50$ in the simulations contained in this work) the method has not converged, a new $\Delta t_{\text{new}} = \Delta t/5$ is tried.

The convergence of the method with the number of nodes in the gas phase and in the liquid phase is checked for an air/vapor bubble of $10 \mu\text{m}$ exposed to a shock wave (further details about the conditions of the simulation can be found in the next section) In these conditions, the bubble behavior is strongly non-linear and a significant gas intake is predicted. As we are interested in the accuracy of the method to predict the growth-rate, the net gas intake after one shock wave is taken as a representative variable of the process. Tables 1 and 2 show that the method converges, but only for a sufficiently large number of nodes in both phases. For the simulations contained in this paper we choose $n_g = n_l = 200$. The tolerance of the iterative solver is set to 10^{-5} and the minimum mesh size, located at the bubble interface is $h_{\min} = 10^{-4}R_0$.

Table 1: Net gas intake as a function of the number of nodes inside the bubble at $t=0.1$ ms (domain size = 5 mm, $n_l = 200$)

n	$m_f/m_0 - 1$
50	0.1179316
100	0.1776510
200	0.1921281
400	0.1949811
800	0.1956019

Table 2: Net gas intake as a function of the number of nodes in the liquid at $t=0.1$ ms (domain size = 5 mm, $n_g = 400$)

n	$m_f/m_0 - 1$
50	0.2056242
100	0.1950348
200	0.1949811
400	0.1949618

4 Numerical examples: Relevant phenomena modelling rectified diffusion

In this section, we discuss the validity of common assumptions used to simulate single bubble dynamics in the context of lithotripsy. In these situations the far field pressure is given by the following expression

$$p_l(t) = p_{\infty} + 2\Delta p \exp(-zt) \cos(\omega t + \pi/3) \quad 0 < t < T \quad (17)$$

where T is the interval between successive pulses. As an example, we take characteristic values for pulses induced in lithotripsy (Church 1988) ($f=83.3$ kHz and $z = 9.1 \cdot 10^5 \text{s}^{-1}$). We consider the case of air/vapor bubbles in water (properties included in Table 3).

The characteristic bubble response is depicted in Figure 1. In general, four different stages can be distinguished. When the wave arrives, the bubble collapses as a response of the sudden increase of pressure. After that,

Table 3: Properties for the liquid and gas used in the simulations contained in this work

Variable	Gas	Liquid	Units
W	28	18	kg mol^{-1}
μ	10^{-5}	10^{-3}	Pas
κ	0.5	0.04	$\text{Wm}^{-1}\text{K}^{-1}$
σ		0.069	Nm^{-1}
D_g	$2.0 \cdot 10^{-9}$	$2.5 \cdot 10^{-4}$	m^2s^{-1}

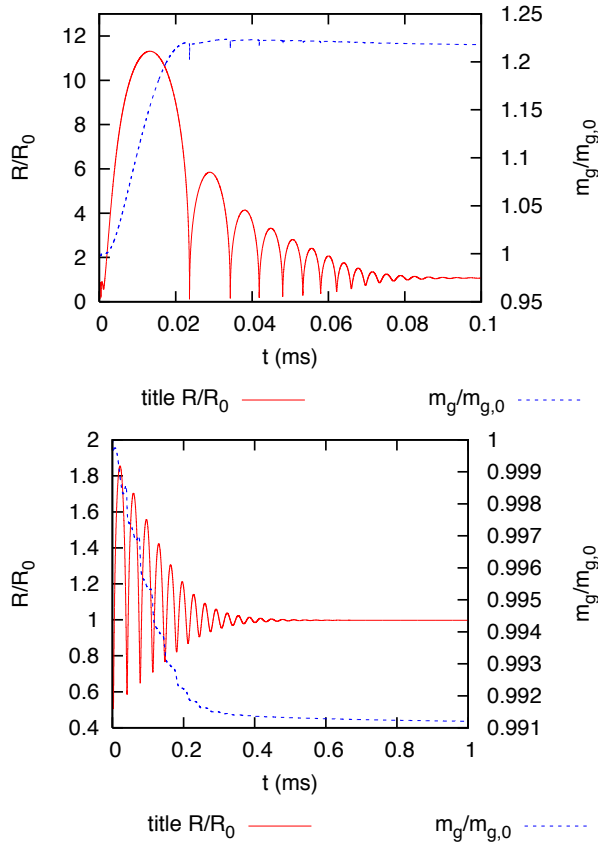


Figure 1: Temporal evolution of the bubble radius and the mass of the bubble for a bubble of 10 μm (up) and 100 μm (bottom) for a wave of 5 MPa. The 10 μm bubble tends to grow due to the large degree of expansion experienced during the tail of the shock wave. As the bubble size increases, the non-dimensional maximum radius decreases, tending to be dissolved.

the negative tail of the wave induced by the lithotripter and the high pressure reached during the first collapse makes the bubble grow.

During this stage, part of the gas dissolved in the liquid is fed into the bubble. The bubble continues its expansion until its pressure falls below the reference pressure and then, the bubble undergoes a series of rebounds until the bubble reaches a mechanical equilibrium with the surrounding liquid. Finally, the bubble tends to dissolve due to the concentration gradient between the interface and the bulk liquid until a new pulse arrives.

4.1 Gas diffusion in the short time scales

In this section we discuss the effects of the short time scales on the process of rectified diffusion.

As it can be seen in Figure 1, most of the gas intake takes part during the expansion process after the initial bubble collapse. Even for the relatively low amplitude tested here, the mass of gas inside a bubble of 10 μm increases by approximately 20 % in each cycle. Once the shock wave has gone away, the bubble equilibrates its pressure with that of the liquid and, due to the concentration gradient between the interface and the bulk liquid, the bubble tends to dissolve. The dissolution rate between the instant when the bubble equilibrates its pressure with the surrounding liquid and the time at which the following bubble arrives, could be computed using the analytical solution found by Epstein and Plesset (1950). However, in saturated liquids the process of dissolution of gas is usually much slower than the repetition frequency of shock waves. Therefore the dissolution between the pressure equilibration and the repetition period T is completely neglected.

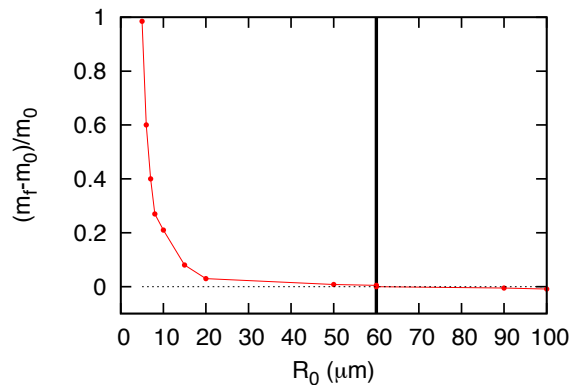


Figure 2: Relative mass increment after the pass of one shock wave as a function of the initial bubble radius for a wave of 5 MPa. The vertical line represents the intersection point (zero growth rate). The relative mass increment diverges as the radius of the bubble decreases. This phenomena is a direct consequence of the sharp boundary layer in the liquid phase which is responsible of the net gas intake during one cycle. The bubbles growth for bubbles of the order of tens of microns is negligible and larger bubbles tend to dissolve.

From Figure 2 we can conclude that the larger the bubble the smaller the relative amount of gas is fed into the bubble. Indeed, we can define a threshold radius,

R_c , which has zero growth rate once the bubble pressure has been equilibrated with that of the liquid. This threshold radius provides an estimation of the value around which the bubble radius distribution should be centered in lithotripsy experiments. Bubbles smaller than R_c grow quickly up to values around R_c , whereas bigger bubbles tend to dissolve (Figure 2).

One of the conclusions of this analysis is that, irrespective of the initial cavitation nuclei distribution of the liquid, after passing some dozens of shock waves the bubble distribution will be centered around values of tens of microns. As it can be seen in Figure 3, this result is not especially sensitive to the pressure wave amplitude and it is in agreement with previous findings by Church (1988); Cunningham et al. (2001). Thus, we can define stability diagrams similar to those of Toegel and Lohse (2003) to determine the values around which the bubble distribution of bubbles tend to be centered.

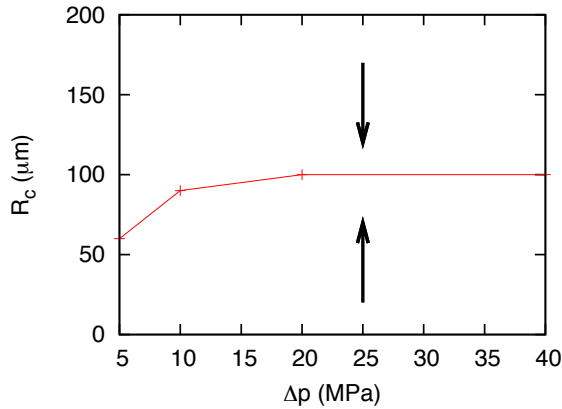


Figure 3: Equilibrium radius as a function of the amplitude of the wave for a wave of $f=83.3$ kHz. For large amplitudes, the equilibrium radius become independent of the pressure wave amplitude

We emphasize that the threshold value in this case is given by the short time scale. Fyrrillas and Szeri (1994) have presented a model to obtain growth rates of bubbles in ultrasonic fields in the long term evolution. One of the main conclusions of their work is that, in ultrasonic applications, the transient effects related during one cycle are irrelevant and the gas intake is only governed by the long time scale. This model has been successfully used to predict the stability ranges in Single Bubble Sonoluminescence by Lohse (Toegel and Lohse 2003). However, the applicability of this model is based on the assumption that the bubble is steadily oscillating, so that the effects on the short time scale have no impact on the long term solution. A simplified expression to work out

the bubble gas intake during one cycle is (Toegel and Lohse 2003):

$$\frac{m_f}{m_0} = 4\pi D_l \frac{R_{\max}}{f} \left(\frac{c_\infty}{c_{\text{sat}}} - \frac{\langle p_i \rangle}{p_\infty} \right) \quad (18)$$

where $\langle p_i \rangle$ is a temporal averaged whose expression is (Toegel and Lohse 2003; Fyrrillas and Szeri 1994)

$$\langle p_i \rangle = \frac{\int_0^T p_i R_b^4 dt}{\int_0^T R_b^4 dt} \quad (19)$$

This expression is problematic when applied to lithotripsy. Firstly, the definition of T is not clear. As a first attempt, one could take T as the inverse of the frequency at which shock waves is induced in the body. However, in this case Eq. 18 would give values of the growth rate that could be make sense, in the most favorable case, over thousand or millions of shock waves.

Then, we can then conclude that the solution of the transport equation of the species α in the liquid is mandatory in processes where the short time scales, of the order of the excitation frequency, control the process. The growth rates of small bubbles can be extremely large even for the small amplitudes tested here, and large bubbles tend to slowly dissolve.

4.2 The influence of mass transfer on the internal bubble profiles

Models assuming uniform properties inside the bubble are widely used in the literature. The validity of the pressure uniformity inside the bubble has been already discussed by (Lin et al. 2002) proving that, even for moderately intense collapses, pressure uniformity holds. Only very intense collapses (Xu et al. 2003) when pressures rise above 10000 atm, and the presence of chemical reactions (Hauke et al. 2007) can induce important pressure gradients during the implosion that must be taken into account in order to accurately describe the bubble implosion.

The variations of other properties like the bubble temperature, density and concentration are usually included in the model by defining averaged values inside the bubble and resorting to different models to obtain the mass and heat transfer fluxes at the interface (Preston et al. 2007; Prosperetti et al. 1988). The simplest models assume that the bubble oscillates around an equilibrium radius. When the mass of gas inside the bubble does not change significantly, the definition of an effective polytropic coefficient and an effective viscosity is usually enough to describe the bubble radius

evolution. However, when the mass of gas during one cycle varies significantly, these models can fail.

When the bubble has a positive mass net flux most of the gas diffusion from the liquid to the bubble is produced during the expansion (e.g. Figure 1a). For an accurate prediction of the gas intake, the main mechanisms influencing the bubble radius and gas intake must be captured.

In this stage, the mass transfer effects play a role on both, the bubble radius evolution as well on the gas diffusion inside the bubble. The evaporation flux across the interface changes the velocity of the interface, significantly modifying the expansion rate. The internal concentration profiles, modify the transport of gas inside the bubble, which ultimately have an impact on the gas intake.

The dimensionless number $J^* = J/(\dot{R}\rho_g)$ is used as a parameter whose absolute value gives us an estimation of the importance of the evaporation flux on the interface velocity, irrespective if condensation or evaporation takes place. For values of J^* much smaller than 1, the flux of mass across the interface has no influence on the interface velocity. For values around one, the mass transfer controls the expansion velocity. As depicted in Figure 4, the evaporation significantly influences the interface velocity during the expansion, therefore, we can conclude that to accurately estimate the maximum radius, a correct prediction of the evaporation flux is required.

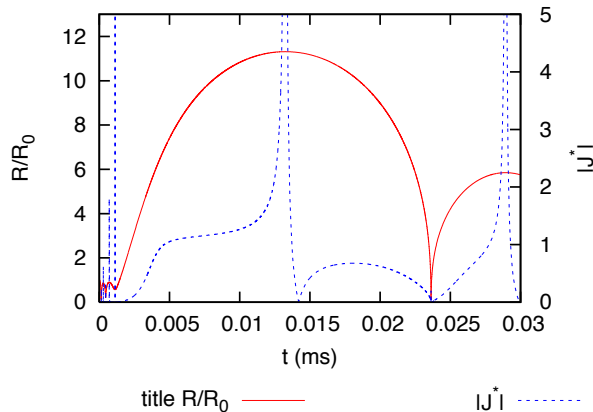


Figure 4: Temporal evolution of the bubble radius and the dimensionless flux J^* for a bubble of $10 \mu\text{m}$ exposed to a shock wave of amplitude 5 MPa. The evaporation flux has an important impact on the expansion velocities when the bubble expands.

The evaporation flux during the expansion is controlled by the diffusion of water vapor inside the bubble. That is, both parameters, the expansion velocity and the diffusive transport of gas inside the bubble, are governed by the diffusion processes inside the bubble. Figure 5 contains the temporal-spatial distribution of water vapor content inside the bubble. Especially during the first stage of the large expansion, when the gas intake is maximum, large concentration gradients inside the bubble are encountered. Whereas the concentration at the interface reaches values around 1, the concentration at the bubble center is around 0.1. These effects are completely missed by models based on uniform properties. Equilibrium conditions are not sustained inside the bubble, only at the interface. Moreover, the large variations on the concentration gradients inside the bubble make it difficult to develop simplified models able to accurately predict the evaporation flux.

Thus, we can conclude that for an accurate prediction of the evaporation flux, the internal concentration gradients must be solved. The evaporation flux controls the diffusion of gas inside the bubble and also the interface velocity during the expansion. Both parameters have an important impact on the predicted growth rates.

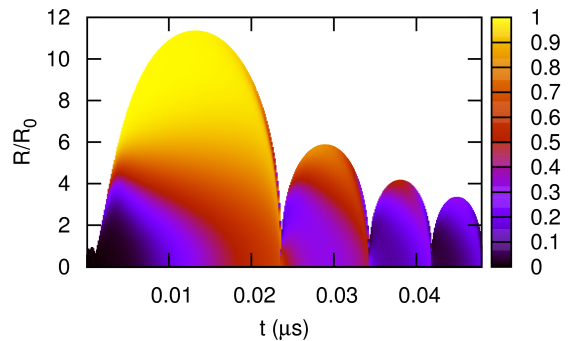


Figure 5: Temporal evolution of the profiles of mass fraction of water vapor inside the bubble for a bubble of $10 \mu\text{m}$ exposed to a shock wave of amplitude 5 MPa. The important internal concentration gradients inside the bubble control the evaporation flux during the expansion processes.

5 Conclusions

A new model for rectified diffusion has been proposed. The current model allows taking into account temperature, concentration and pressure gradients both inside

and outside the bubble.

In the context of lithotripsy, the growth rate of the bubbles is shown to depend significantly on the transport of gas in the liquid in a time scale of the order of the pulsating frequency.

The simulations reveal that irrespective to the initial bubble distribution, bubbles present in the liquid will tend to quickly reach an equilibrium radius of the order of tens of microns. This conclusion should be relevant for the radius distribution used for the analysis of the effects of cavitation in lithotripsy.

The inclusion of liquid vaporization has an important role for an accurate prediction of the growth rates, especially for bubbles of the order of microns. The mass transport related with the liquid phase change influences the expansion velocity. The evaporation and condensation flux is given by the vapor diffusion rate inside the bubble. Thus, it is required to compute the species concentration gradient inside the bubble for an accurate prediction of the gas intake.

Acknowledgements

The authors would like to acknowledge the comments and suggestions of Dr. Tim Colonius and also Dr. Cesar Dopazo and Dr. Guillermo Hauke for their support.

References

- F.G. Blake Jr. Onset of Cavitation in Liquids. *Thesis (Ph. D.)—HARVARD UNIVERSITY, 1949*. Source: *American Doctoral Dissertations, Source code: W1949.*, page 0049, 1949.
- C. Brennen. *Cavitation and Bubble Dynamics*. Oxford University Press, New York. ISBN 0195094093, 1995.
- C.C. Church. A theoretical study of cavitation generated by an extracorporeal shock wave lithotripter. *J. Acoust. Soc. Am.*, 83:572, 1988.
- L.A. Crum. Measurements of the growth of air bubbles by rectified diffusion. *J. Acoust. Soc. Am.*, 68:203, 1980.
- K.B. Cunningham, A.J. Coleman, T.G. Leighton, and P.R. White. Characterising in vivo acoustic cavitation during lithotripsy with time-frequency methods. *Acoustics Bulletin*, 26(5):10–16, 2001.
- A. Eller and H.G. Flynn. Rectified diffusion during non-linear pulsations of cavitation bubbles. *J. Acoust. Soc. Am.*, 37:493, 1965.
- A.I. Eller. Growth of bubbles by rectified diffusion. *J. Acoust. Soc. Am.*, 46:1246, 1969.
- P.S. Epstein and M.S. Plesset. On the Stability of Gas Bubbles in Liquid-Gas Solutions. *J. Chem. Phys.*, 18:1505, 1950.
- M.M. Fyrrillas and A.J. Szeri. Dissolution or growth of soluble spherical oscillating bubbles. *J. Fluid Mech.*, 277:381–407, 1994.
- Y. Hao and A. Prosperetti. The dynamics of vapor bubbles in acoustic pressure fields. *Phys. Fluids*, 11(8):2008–2019, 1999.
- G. Hauke, D. Fuster, and C. Dopazo. Dynamics of a single cavitating and reacting bubble. *Phys. Rev. E*, 75(066310):1–14, 2007.
- S. Hilgenfeldt, D. Lohse, and M.P. Brenner. Phase diagrams for sonoluminescing bubbles. *Phys. Fluids*, 8:2808–2826, 1996.
- D.Y. Hsieh and M.S. Plesset. Theory of rectified diffusion of mass into gas bubbles. *J. Acoust. Soc. Am.*, 33:206, 1961.
- J. Keller and M. Miksis. Bubble oscillations of large amplitude. *J. Acoust. Soc. Am.*, 68(2):628–633, 1980.
- H. Lin, B. D. Storey, and A. J. Szeri. Inertially driven inhomogeneities in violently collapsing bubbles: the validity of the rayleigh-plesset equation. *J. Fluid Mech.*, 452:145–162, 2002.
- W.H. Press, S.A. Teukolsky, W.T. Vetterling, and B.P. Flannery. *Numerical Recipes in Fortran 77*. Press Syndicate of the university of Cambridge, The Pitt Building, Trumpington Street, Cambridge CB2 1RP, 1992.
- A.T. Preston, T. Colonius, and C.E. Brennen. A reduced order model of diffusive effects on the dynamics of bubbles. *Phys. of Fluids*, 19(123302):1–19, 2007.
- A. Prosperetti, L.A. Crum, and K.W. Commander. Non-linear bubble dynamics. *J. Acoust. Soc. Am.*, 83:502–514, 1988.
- S. Sochard, A.-M. Wilhelm, and H. Delmas. Gas-vapour bubble dynamics and homogeneous sonochemistry. *Chem. Eng. Sci.*, 53(2):239–254, 1998.
- B. D. Storey and A.J. Szeri. Water vapour, sonoluminescence and sonochemistry. *Proc. R. Soc. Lond. A*, 456:1685–1709, 2000.
- R. Toegel and D. Lohse. Phase diagrams for sonoluminescing bubbles: A comparison between experiment and theory. *J. Chem. Phys.*, 118(4):1863–1875, 2003.

N. Xu, R.E. Apfel, A. Khong, X. Hu, and L. Wang. Water vapor diffusion effects on gas dynamics in a sonoluminescing bubble. *Phys. Rev. Lett. E*, 68(016309):1–7, 2003.

K. Yasui. Alternative model of single sonoluminescence. *Phys. Rev. E*, 56(6):6750–6760, 1997.